Optical and magnetic properties in epitaxial GdN thin films

Yoshitomi, Hiroaki ; Kitayama, Shinya ; Kita, Takashi ; Wada, Osamu ; M. Fujisawa ; Ohta, Hitoshi ; T. Sakurai

(Citation)
Physical Review B,83(15):155202-155202

(Issue Date)
2011-04-08

(Resource Type)
journal article

(Version)
Version of Record

(URL)
https://hdl.handle.net/20.500.14094/90001367

Optical and magnetic properties in epitaxial GdN thin films

H. Yoshitomi, S. Kitayama, T. Kita, and O. Wada
Department of Electrical and Electronic Engineering, Graduate School of Engineering, Kobe University, 1-1 Rokkodai, Kobe 657-8501, Japan

M. Fujisawa and H. Ohta
Molecular Photoscience Research Center and Graduate School of Science, Kobe University, 1-1 Rokkodai, Kobe 657-8501, Japan

T. Sakurai
Center for Support to Research and Education Activities, Kobe University, 1-1 Rokkodai, Kobe 657-8501, Japan
(Received 26 February 2010; revised manuscript received 26 January 2011; published 8 April 2011)

We studied the optical and magnetic properties in epitaxial AlN/GdN/AlN double heterostructures grown using reactive sputtering under ultrapure conditions. The indirect and direct optical transitions in a 95-nm-thick GdN film were found to be 0.95 and 1.18 eV, respectively. The considerable size effects of the optical band gap were observed with a decrease in the GdN thickness. The AlN/GdN/AlN double heterostructures clearly exhibited ferromagnetic states at low temperature. The short-range correlation of spins began to develop below ∼60 K, and long-range ordering that obeyed the Arrott relation was confirmed below ∼30 K. Because of the film-size independence for the ferromagnetic ordering, the cooperative correlation length in GdN was considered to be shorter than 30 nm. Furthermore, we found that the band gap is dramatically reduced with the ferromagnetic spin ordering.

DOI: 10.1103/PhysRevB.83.155202 PACS number(s): 75.50.Pp, 71.20.Eh, 75.50.Gg, 78.20.−e

Spintronics, which is based on current semiconductor technologies, originated from the physics involved in magnetic semiconductors. Compounds and alloys of rare-earth (RE) semiconductors are intrinsically magnetic semiconductors; RE elements with open 4*f* shells create enormously enhanced magnetic moments.[1–10] GdN is known to have a moment of $7\mu_B$/Gd and is ferromagnetic. Although the strong ferromagnetism in GdN affects its performance as a magnetic semiconductor, the electronic structure influencing the ferromagnetism is still being investigated.[6–10] Clearly, it is important to understand the credible band structure of high-quality GdN crystals. On the other hand, nitride-based semiconductors have recently been widely used in novel devices such as light-emitting diodes, laser diodes, and high electron mobility transistors for realizing high-power operation.[12–14] The combination of current nitride semiconductor systems with nitride-based magnetic semiconductors will open a new field of novel spintronic devices.

GdN is known to exhibit ferromagnetism because of its fully occupied 4*f*-electronic states.[2–10] The Curie temperature (T_c) of unstrained bulk GdN has been reported to be around 70 K.[2–5] The lattice extension reduces the magnetization and decreases T_c to 20 K.[3] On the other hand, in the presence of partially filled Gd-4*f* states, the exchange interaction shifts the spin-split conduction and valence-band edges in the opposite direction: the majority-spin gap is reduced while the minority-spin gap becomes wide.[8] The band structure of GdN has been widely studied theoretically[6–8] and experimentally.[4,5,9–11] Lambrecht predicted that the GdN was an indirect band-gap semiconductor with a gap of 0.7–0.85 eV and 1.1–1.2 eV for the indirect and direct gaps, respectively.[6] In order to explain published legacy experimental data,[11] they updated the results tuned by using the same calculation method as performed in Ref. 6, which results in the indirect and direct gaps of 0.69 and 0.98 eV, respectively.[7] Recently, a ferromagnetic redshift of the optical band gap has been reported for a high-quality GdN thin film with 200 nm thickness,[9] where an unambiguous signature of the direct gap at the *X* point was observed at 1.3 eV in the paramagnetic phase at 300 K. They also performed theoretical calculations by reconsidering computational treatment of the Gd 4*f* level. The updated results for the indirect and direct gaps are 0.98 and 1.30 eV, respectively. Thus, the direct gap is in exact agreement with the included experimental results, though the indirect band gap is still unclear. Thus, precise experimental demonstration of the band-edge structure is indispensable. Furthermore, size effects caused by the thin-film structures on the optical and magnetic properties should be understood in order to apply GdN to nitride-based spintronic applications.

In this work, we studied the band-edge structure of AlN/GdN/AlN double heterostructures with GdN thicknesses of less than 95 nm. Indirect and direct optical transitions were clearly confirmed. The AlN/GdN/AlN double heterostructures exhibited ferromagnetic ordering below ∼30 K. We discuss the size effects on the optical and magnetic properties in detail in this paper.

Double heterostructures of AlN/GdN/AlN were used in this study to avoid oxidation.[15] All samples used were grown on sapphire (0001) substrates at 500 °C by reactive radio-frequency (RF) magnetron sputtering[16] in an ultrahigh vacuum chamber with a base pressure of approximately 6×10^{-6} Pa. The growth chamber equipped with multitargets for AlN and GdN was separated from the substrate introduction chamber to avoid oxidation of the target when introducing the substrate. Al (99.99%) and Gd (99.9%) were used as metal targets. We used an ultrapure (99.9999%) gas mixture of argon and nitrogen for reactive growth, and the partial pressure ratio was even. The total sputtering pressure was 5 Pa. The input RF power was

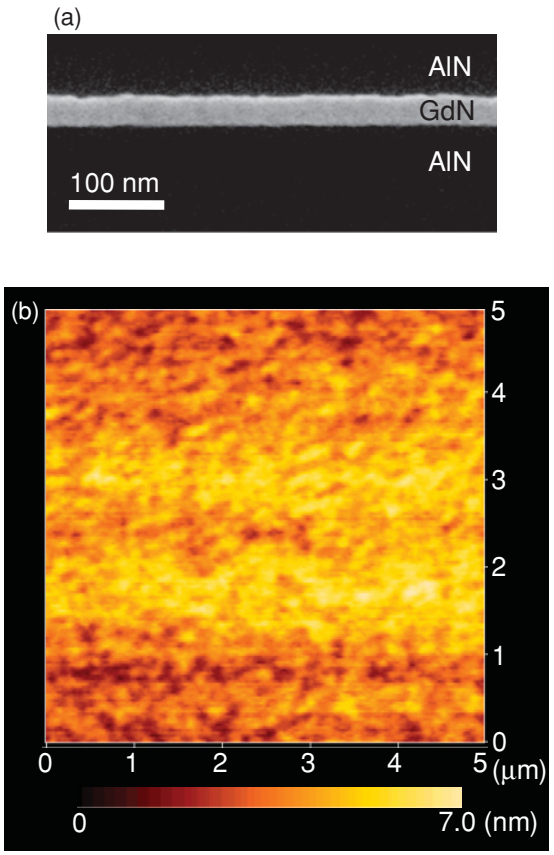

FIG. 1. (Color online) (a) SEM cross-sectional image of an AlN/GdN (30 nm)/AlN double heterostructure. (b) AFM image in $5 \times 5\ \mu m^2$ of the film.

250 W. First, a 100-nm-thick AlN-buffer layer was deposited on the substrate. The GdN layer was grown on the buffer layer. Finally, the surface was capped by a 100-nm-thick layer of AlN. The thickness of the GdN thin layer was changed from 30 to 95 nm.

The crystallographic structure was characterized by x-ray diffraction (XRD), extended x-ray absorption fine structure (EXAFS) analysis, and transmission-electron microscopy (TEM). Oxygen content in the film was studied by secondary-ion mass spectrometry (SIMS). A scanning electron microscope (SEM) was employed to study the morphology of the heterointerfaces of the double heterostructures. Furthermore, atomic force microscopy (AFM) was applied to investigate the wide range flatness of the film. The band-edge structures were investigated by optical absorption spectra. The absorption spectra were obtained in the range of 200–2500 nm using a spectrophotometer (Hitachi High-Tech U-4100). In order to investigate the fundamental magnetic properties of GdN, magnetization measurements were carried out down to $T = 2$ K in magnetic fields up to $B = 5$ T using a superconducting quantum interference device magnetometer (Quantum Design MPMS XL). The magnetic field was applied along the in-plane orientation.

The interfaces of the double heterostructures were investigated by the cross-section SEM. The observed SEM image is shown in Fig. 1(a). Clear and flat interfaces were confirmed even for the double heterostructure with the thinnest GdN

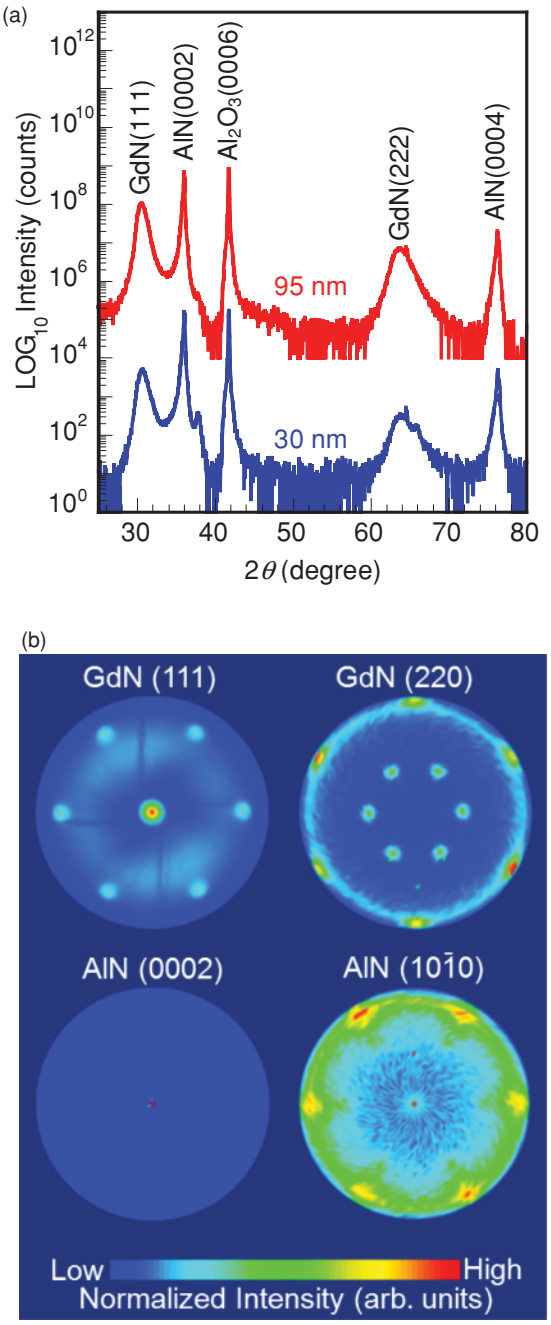

FIG. 2. (Color online) (a) X-ray diffraction spectra for AlN/GdN/AlN double heterostructures with 30- and 95-nm-thick GdN. (b) X-ray pole figures of in and out planes of AlN and GdN.

layer of 30 nm. A slight fluctuation of less than ~4.0 nm at the heteroboundary was due to the surface morphology of the AlN-buffer layer. The surface morphology in the wide range of the film was investigated by AFM observations. A typical AFM image in $5 \times 5\ \mu m^2$ is shown in Fig. 1(b). The roughness in the height was less than 4.40 nm, which was almost the same as the fluctuation of the heterointerface observed by the cross-section SEM in Fig. 1(a), and the root-mean-square roughness was approximately 0.62 nm at this area. We carried out x-ray diffraction measurements. Figure 2(a) shows x-ray diffraction spectra of the AlN/GdN/AlN double heterostructures with

30- and 95-nm-thick GdN. The diffraction signals from the GdN layer indicate the ⟨111⟩ preferential orientation of the rocksalt structure on the *c*-axis-oriented AlN with the wurtzite structure. X-ray pole figures of the in and out planes of AlN and GdN are shown in Fig. 2(b). The pole figure of AlN exhibits a strong *c*-axis orientation and the sixfold symmetry consisting with the symmetry of the wurtzite crystal structure. On the other hand, the signal of planes of GdN also shows the sixfold symmetry, whereas the rocksalt structure should have the threefold symmetry if the film is a single crystal. This result indicates the formation of antiphases of GdN in the (111) plane.[5] Thus, it is concluded that our double heterostructures of AlN/GdN/AlN were expitaxially grown on the sapphire (0001) substrate. From analyzing the diffraction spectra, the lattice space in the growth direction for 30- and 95-nm-thick GdN were 0.291 and 0.292 nm, respectively. These values are slightly larger than the 0.289 nm recorded for bulk GdN.[17] A similar phenomenon was confirmed for the AlN layer. The lattice expansion along the growth direction may have been due to the thermal expansion mismatch between the grown film and sapphire substrate. The thermal-expansion coefficient 4.4×10^{-6} K^{-1} for AlN was slightly smaller than that for sapphire (7.0×10^{-6} K^{-1}). This caused a biaxial compressive strain in the AlN/GdN/AlN double heterostructure, and thus the lattice space in the growth direction is expanded. In this study, we neglected the influence of the thin GdN layer on the thermal expansion mismatch. Actually, the in-plane x-ray diffraction spectrum indicated that the lattice space was reduced; the value of the ⟨200⟩ direction for 95-nm-thick GdN was 0.249 nm while that for the bulk GdN was 0.250 nm.[17] These results are different from a recent report[18] where the in-plane lattice constant was enlarged for thin films and decreased with the increase in the film thickness due to an oxygen contamination. According to the relations observed for the lattice spaces of both the growth and in-plane directions, we consider that there is no effect of oxygen contamination. Our samples grown under ultrapure conditions do not show any signs of oxygen contamination. The radial structure functions around Gd ions in the AlN/GdN/AlN double heterostructures were studied by analyzing EXAFS signals (Fig. 3). The structure function for GdN clearly exhibited the nearest-neighbor sites of nitrogen, the second-nearest sites of the next Gd, and the third-nearest sites of the next nitrogen. We found no signals related to Gd_2O_3 and metal Gd. We also performed SIMS measurements to clarify how much oxygen is contained in our films. Figure 4 shows a typical depth profile of the secondary-ion intensity obtained for an AlN/GdN multilayered structure. The dashed line indicates a level of 1.0×10^{20} cm^{-3} of oxygen content in the AlN region. Oxygen is a well-known impurity in AlN crystals. The oxygen content of bulk AlN was reported to be approximately 1×10^{19} cm^{-3} even in the lowest impurity level.[19,20] The SIMS analysis also showed evidence of oxygen in GdN. The secondary-ion intensity in GdN was confirmed to be one order larger than that in AlN. This result gives us an impression that the oxygen content in GdN seems to be higher than that in AlN. However, the oxygen content is impossible to estimate from the secondary-ion intensity profile without using the ionization efficiency in AlN and GdN. We have data of the ionization efficiency in AlN, but there is no information about that of impurities in GdN. Therefore,

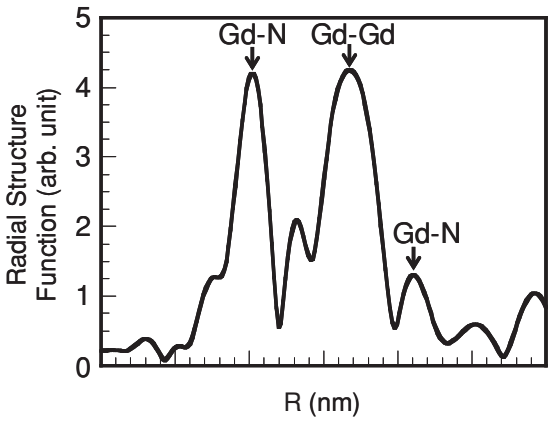

FIG. 3. Radial structure functions around Gd ions in 95-nm-thick GdN.

the exact value of the oxygen concentration in GdN was, unfortunately, unable to be estimated.[21] At this moment, it is unclear whether the strong secondary-ion intensity in GdN indicates a high oxygen concentration or not.

Figure 5(a) shows optical absorption spectra of the samples with 30-, 59-, and 95-nm-thick GdN. In our measurements, an inhomogeneous background can be negligible because the background was canceled by subtracting a transmitted signal passing through a reference sapphire substrate. Here, wemust note an interference effect superimposed on the absorption spectrum. Figure 5(b) shows a typical comparison between the absorption spectrum of 30-nm-thick GdN and a calculated multiple interference spectrum of the double heterostructure formed on the sapphire substrate. In this calculation, we do not include an absorption profile around the fundamental band edge in order to make clear the contribution of the interference effect on the spectrum. The interference signal was observed clearly in the visible region less than 500 nm. The calculated interference structure moderately reproduces the complicated

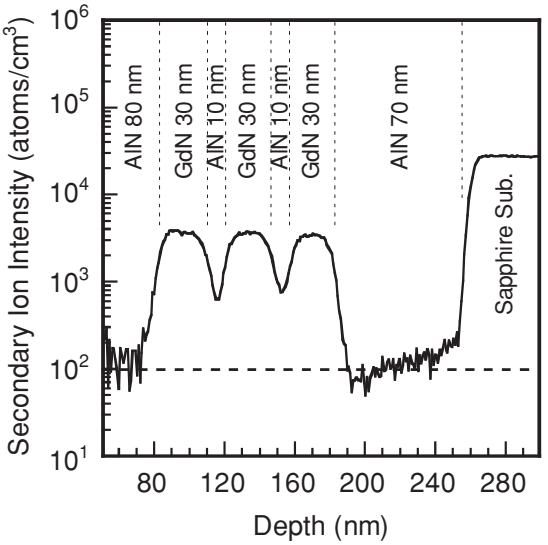

FIG. 4. A typical depth profile of the secondary-ion intensity obtained for an AlN/GdN multilayered structure. The dashed line indicates a level of 1.0×10^{20} cm^{-3} of the oxygen content in AlN.

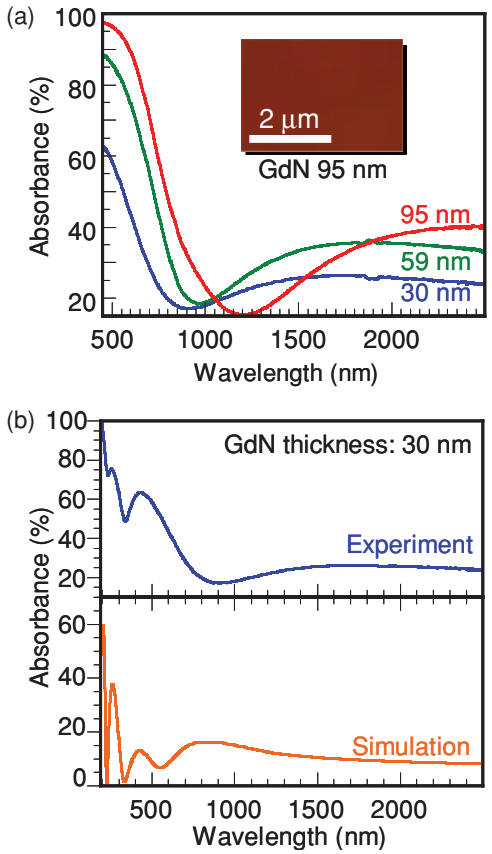

FIG. 5. (Color online) (a) Absorption spectra of double heterostructures with 95-, 59-, and 30-nm-thick GdN. The inset is a transmitted optical photomicrograph of the AlN/GdN (95 nm)/AlN heterostructure. (b) Comparison of an absorption spectrum of 30-nm-thick GdN and a calculated spectrum.

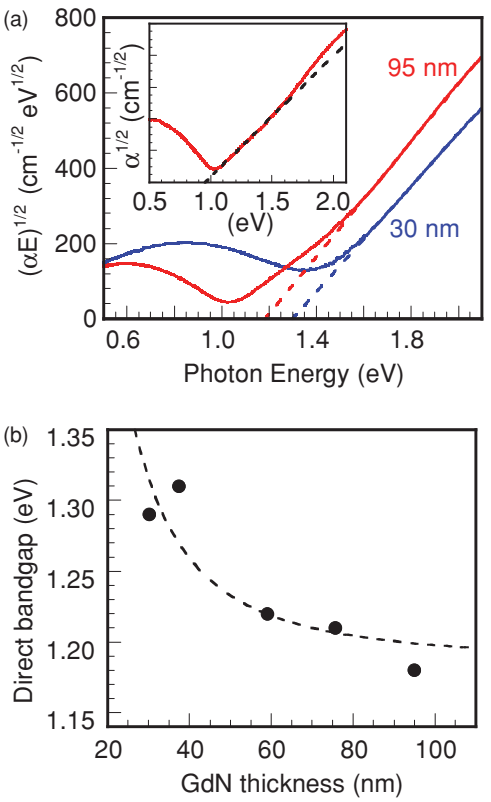

FIG. 6. (Color online) (a) Tauc plots $(\alpha E)^{1/2}$ for heterostructures with 95- and 30-nm-thick GdN. Dashed lines indicate linear dependences for $(\alpha E)^{1/2}$. The inset is an analysis of the indirect band edge for 95-nm-thick GdN, and the dashed line indicates a linear dependence of $\alpha^{1/2}$. (b) Direct transition energies estimated by the Tauc plot as a function of the GdN thickness. The dashed line indicates a fitting curve representing a d^{-2} dependence.

structure observed in the absorption spectrum. According to these results, it is found that the interference signal gently changes around the band edge and the influence to the absorption profile is negligible below the band edge. Thus, we analyzed the band edges using the observed absorption spectra shown in Fig. 5(a). All of the absorption spectra exhibited clear absorption edges around 1000 nm. These results support the argument that GdN thin films are semiconductors.[6–9,11] The inset shows a transparent optical microscope image of the sample with 95-nm-thick GdN. The transparent color is red-brown. A significant broad absorption signal related to free carriers that may have been supplied by nitrogen vacancies[4,10] appears at the longer wavelength side below the band gap. With a decrease in the GdN thickness, the peak position of the free-carrier absorption shifted toward the shorter wavelength side while the intensity decreased. According to the Drude model,[22] the plasma frequency is proportional to the carrier density. Therefore, the observed results indicate that the free-carrier density in the double heterostructure with thinner GdN layer was high and that the total number of carriers became large in the thicker film.

The fundamental absorption edge was found to clearly depend on the GdN-layer thickness. When the thickness was decreased, the band gap widened. The direct band-gap energy at the X point was estimated by the Tauc plot,[23] as shown in Fig. 6(a) for samples with 30- and 95-nm-thick GdN. The Tauc plot is an analysis method that estimates the direct band gap of semiconductors with fluctuating potentials. The plot of the absorption signal indicates a linear dependence. Dashed lines guide the linear dependence, and the zero-cross energy corresponds to the direct band edge. The estimated direct band gaps of 30- and 95-nm-thick GdN were approximately 1.29 and 1.18 eV, respectively. Figure 6(b) shows the GdN-thickness (d) dependence of the estimated direct transition energy. The direct transition energy demonstrated considerable blue shifts as d decreased; this may be due to the quantum size effect on the band gap. The dashed line represents a d^{-2} dependence. If we assume an infinite barrier for the GdN quantum well—which is a reasonable assumption because of the large band-gap difference between AlN (6.2 eV) (Ref. 24) and GdN (1.2 eV)—the reduced effective mass can be estimated to be less than $0.01m_0$. The reason for such small effective mass when compared with well-known nitride semiconductors is under investigation. We may have to note the Burstein-Moss shift caused by excess carriers provided by nitrogen vacancies to interpret the band-gap change.[25]

On the other hand, the fundamental absorption edge of GdN was predicted to be indirect.[6,7] The Tauc plot of the 95-nm-thick sample deviated from the linear dependence

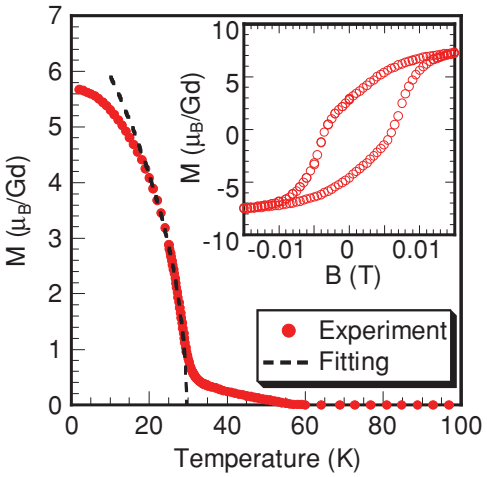

FIG. 7. (Color online) Magnetization of 95-nm-thick GdN at $B = 2.0$ mT is shown as a function of temperature. Magnetic field was applied in the plane. A broken line represents a fitting curve. The inset shows the magnetization of 95-nm-thick GdN at 4.2 K.

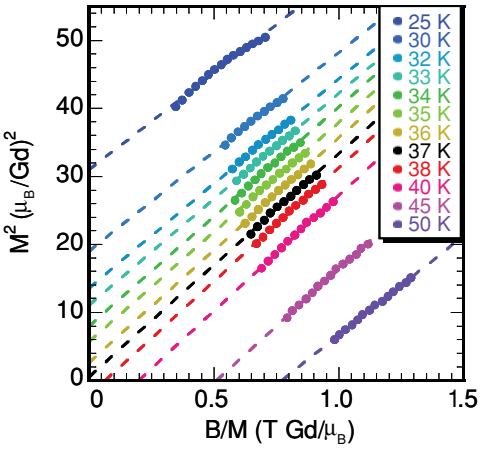

FIG. 8. (Color online) Arrott plot of M^2 versus B/M for 95-nm-thick GdN at various temperatures. Magnetic field was applied in the plane. Broken lines indicate extrapolations of experimental data.

below ~1.5 eV. This may have been due to indirect absorption. The indirect band-gap energy can be estimated by analyzing $\alpha^{1/2}$. The inset in Fig. 6(a) shows the result. The $\alpha^{1/2}$ plot agrees well with a linear dependence in this region, which demonstrates that the transition is indirect. The estimated indirect band gap was 0.95 eV, which is close to the theoretically calculated value.[6,7] The indirect absorption of 95-nm-thick GdN was clearly observed. However, the indirect edge of the thinner GdN film could not be clearly resolved because of the strong free-carrier absorption caused by the relatively high carrier density.

Figure 7 shows the magnetization of the AlN/GdN/AlN double heterostructure with 95-nm-thick GdN at $B = 2.0$ mT as a function of temperature. When the temperature decreased to below 60 K, the magnetization began to gradually increase. This behavior, which is often observed in ferromagnets, indicates that the short-range correlation of spins, and not the long-range ferromagnetic ordering, begins to develop around 60 K. With further decreases in the temperature, the magnetization increased drastically below 30 K and reached saturation near 5 K. This rapid increase in magnetization was caused by the phase transition from the paramagnetic state to ferromagnetic. With the temperature approaching zero, the magnetization was saturated ~$6\mu_B/Gd^{3+}$ at $B = 2.0$ mT. This value is slightly smaller than the theoretically expected value of $7\mu_B/Gd^{3+}$. This can be interpreted by a magnetic anisotropy induced by the crystal symmetry and/or macroscopic shape, and/or influences caused by the external magnetic field. An hysteresis loop of magnetization of 95-nm-thick GdN at $T = 4.2$ K is shown in the inset of Fig. 7. The magnetization saturates around 0.5 T. The coercive field was less than 0.01 T as shown in the inset of Fig. 7. Thus, 95-nm-thick GdN is considered to be behaving as a *soft* ferromagnetic material. The sample with 30-nm-thick GdN also exhibited similar behavior. According to the simple mean-field theory, the magnetization of ferromagnets vanishes according to the relationship $(T_c\text{-}T)^{1/2}$, where temperature T approaches T_c from $T < T_c$. By using this formula and the data points for 95- and 30-nm-thick GdN between $T = 20$ and 28 K, the best fits were obtained when $T_c = 29.5 \pm 1.0$ and 32.5 ± 1.0 K, respectively. However, these fittings also had some ambiguities when determining T_c. In the ferromagnetism field, the best way to determine T_c is to employ the Arrott plot, which plots M^2 against B/M.[26] According to the mean-field theory of ferromagnets, M^2 vs B/M at various temperatures should show a series of parallel lines near T_c. Since the line at $T = T_c$ should cross the origin, we can determine T_c without ambiguity.

Figure 8 shows an Arrott plot of 95-nm-thick GdN at various temperatures. The broken lines indicate extrapolation lines of experimental data. From these extrapolation lines, we estimated T_c for both 95- and 30-nm-thick GdN to be 37 ± 1 K. It is noted that this value is close to a theoretical calculation obtained by using the Monte Carlo simulation,[27] although the result is considerably smaller than those of previous experimental studies, e.g., $T_c = 68$, 69, or 58 K as estimated by Granville *et al.*,[4] Khanzen *et al.*,[3] and Leuenberger *et al.*,[10] respectively. The differences of these experimental results may be attributed to differences in the stoichiometry, film thickness, and grain size. In addition, when a gradual (not rapid) increase of magnetization is caused by the development of a short-range correlation between spins, the temperature may be regarded as T_c in previous studies. Furthermore, the uniaxial expansion in the growth direction, which is caused by the biaxial compressive strain in the GdN thin layer, is considered to lead a change in T_c.[3,28] We emphasize that the Arrott plot is required for accurately determining T_c. We note that the estimated T_c was almost independent of the GdN-layer thickness in the range of 30–95 nm, while the optical band gap exhibited considerable size dependence. This result indicates that the correlation length between spins was shorter than 30 nm. Furthermore, the magnetization curve as shown in Fig. 7 was also independent of the GdN-layer thickness in the range of 30–95 nm, while the carrier density was found to increase with the decrease in the GdN thickness. This indicates that the origin of the ferromagnetism in the GdN film is insensitive to the carrier density. Thus it is considered that the mechanism of the ferromagnetism can be attributed not to

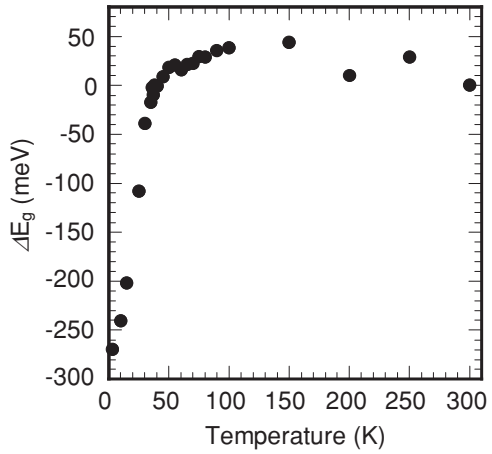

FIG. 9. Temperature dependence of the direct band-gap energy of 95-nm-thick GdN. ΔE_g corresponds to the change in the band-gap energy versus the room-temperature value.

the RKKY interaction depending on carrier density, but to the superexchange interaction.[27]

Finally, we focus on magneto-optical effects observed in the AlN/GdN/AlN double heterostructure. Figure 9 shows the temperature dependence of the direct band-gap energy of 95-nm-thick GdN. With the decrease in the temperature, a slight blue shift against the room-temperature band gap was observed in the high-temperature region. This is a well-known semiconducting nature.[29] With the temperature approaching the T_c, the band gap starts to reduce gradually, which corresponds to the development of the short-range correlation of spins. Finally, below the T_c, the band gap has been found to show a dramatic reduction due to the long-range ferromagnetic ordering of spins. The band gap reduces approximately 300 meV below the T_c. These features appeared in the band gap and agree well with the change in the magnetization as shown in Fig. 7. Therefore, this remarkable redshift is considered to be due to the ferromagnetic ordering of spins in the lower energy state, which is the majority spin band[8,9] according to the Hund's rule. This is an important feature of the intrinsic magnetic semiconductor, and such a phenomenon cannot be observed in the diluted magnetic semiconductors.

In summary, optical band-edge structures of epitaxial AlN/GdN/AlN double heterostructures grown on sapphire (0001) plane were studied. We observed a clear absorption edge in the near infrared region with significant free-carrier absorption below the band gap. The indirect transition (0.95 eV) between the valence-band maximum at the Γ point and the conduction-band minimum at the *X* point was confirmed together with the strong direct optical transition of 1.18 eV at the *X* point for a relatively thick GdN layer of 95 nm. The optical band gap was found to widen with a decrease in the GdN thickness. The short-range correlation between spins in the AlN/GdN/AlN double heterostructures was observed to start developing below ∼60 K, and a clear cooperative ferromagnetic ordering obeying the Arrott relation was confirmed below ∼30 K. Such ferromagnetic ordering is almost independent of the film thickness in the range from 30 to 95 nm. Because of this, the cooperative correlation length in GdN is considered to be shorter than 30 nm. Furthermore, we found that the band gap is dramatically reduced with the ferromagnetic spin ordering, which agreed well with the variation of the magnetization.

ACKNOWLEDGMENTS

The authors would like to thank T. Ishihara for making x-ray pole figure measurements and M. Ogawa for fruitful discussions about the electronic band structure of GdN. M.F. and H.O. would like to thank H. Kato for valuable discussions about the measurement of ferromagnetism. This work was partly supported by Grant-in-Aid for Creative Science Research (No. 19GS1209) from Japan Society for the Promotion of Science (JSPS).

[1] S. Dhar, O. Brandt, M. Ramsteiner, V. F. Sapega, and K. H. Ploog, Phys. Rev. Lett. **94**, 037205 (2005).
[2] G. Busch, J. Appl. Phys. **38**, 1386 (1967).
[3] K. Khazen, H. J. von Bardeleben, J. L. Cantin, A. Bittar, S. Granville, H. J. Trodahl, and B. J. Ruck, Phys. Rev. B **74**, 245330 (2006).
[4] S. Granville, B. J. Ruck, F. Budde, A. Koo, D. J. Pringle, F. Kuchler, A. R. H. Preston, D. H. Housden, N. Lund, A. Bittar, G. V. M. Williams, and H. J. Trodahl, Phys. Rev. B **73**, 235335 (2006).
[5] M. A. Scarpulla, C. S. Gallinat, S. Mack, J. S. Speck, and A. C. Gossard, J. Cryst. Growth **311**, 1239 (2009).
[6] W. R. L. Lambrecht, Phys. Rev. B **62**, 13538 (2000).
[7] P. Larson, W. R. L. Lambrecht, A. Chantis, and M. van Schilfgaarde, Phys. Rev. B **75**, 045114 (2007).
[8] C. Mitra and W. R. L. Lambrecht, Phys. Rev. B **78**, 195203 (2008).
[9] H. J. Trodahl, A. R. H. Preston, J. Zhong, B. J. Ruck, N. M. Strickland, C. Mitra, and W. R. L. Lambrecht, Phys. Rev. B **76**, 085211 (2007).
[10] F. Leuenberger, A. Parge, W. Felsch, K. Fauth, and M. Hessler, Phys. Rev. B **72**, 014427 (2005).
[11] L. F. Schneemeyer, J. Appl. Phys. **61**, 3543 (1981).
[12] P. Ruterana, M. Albrecht, and J. Neugebauer, *Nitride Semiconductors: Handbook on Materials and Devices* (Wiley-VCH, Weinheim, 2003).
[13] I. Akasaki and H. Amano, Jpn. J. Appl. Phys. **45**, 9001 (2006).
[14] H. Morkoç, *Handbook of Nitride Semiconductors and Devices* (Wiley-VCH, Weinheim, 2008), Vol. 3.
[15] W. C. Koehler, J. Appl. Phys. **41**, 933 (1970).
[16] A. Kishimoto, Y. Inou, T. Kita, and O. Wada, Phys. Status Solidi C **4**, 2490 (2007).
[17] L. G. Berry, *Powder Diffraction File* (Joint Committee on Powder Diffraction Standards, Pennsylvania, 1972).
[18] B. M. Ludbrook, I. L. Farrell, M. Kuebel, B. J. Ruck, A. R. H. Preston, H. J. Trodahl, L. Ranno, R. J. Reeves, and S. M. Durbin, J. Appl. Phys. **106**, 063910 (2009).

[19]V. Noveski, R. Schlesser, B. Raghothamachar, M. Dudley, S. Mahajan, S. Beaudoin, and Z. Sitar, J. Cryst. Growth **279**, 13 (2005).
[20]M. Bickermann, B. M. Epelbaum, and A. Winnacker, J. Cryst. Growth **269**, 432 (2004).
[21]J. W. Gerlach, J. Mennig, and B. Rauschenbach, Appl. Phys. Lett. **90**, 061919 (2007).
[22]H. B. Briggs and R. C. Fletcher, Phys. Rev. **91**, 1342 (1953).
[23]J. Tauc, *Amorphous and Liquid Semiconductors* (Plenum, London, 1974).
[24]T. Kita, S. Kitayama, M. Kawamura, O. Wada, Y. Chigi, Y. Kasai, T. Nishimoto, H. Tanaka, and M. Kobayashi, Appl. Phys. Lett. **93**, 211901 (2008).
[25]E. Burstein, Phys. Rev. **93**, 632 (1954).
[26]A. Arrott, Phys. Rev. **108**, 1394 (1957).
[27]C. G. Duan, R. F. Sabiyanov, W. N. Mei, P. A. Dowben, S. S. Jaswal, and E. Y. Tsymbal, Appl. Phys. Lett. **88**, 182505 (2006).
[28]C. G. Duan, R. F. Sabiryanov, J. Liu, W. N. Mei, P. A. Dowben, and J. R. Hardy, Phys. Rev. Lett. **94**, 237201 (2005).
[29]Y. P. Varshni, Physica **34**, 149 (1967).